ACS OMEGA

Open Access

http://pubs.acs.org/journal/acsodf

Article

Controlled PVA Release from Chemical−Physical Interpenetrating Networks to Treat Dry Eyes

Piyush Garg, Parvin Shokrollahi, Haile Fentahun Darge, Chau-Minh Phan, and Lyndon Jones*

Cite This: *ACS Omega* 2025, 10, 1249−1260

Read Online

ACCESS | Metrics & More | Article Recommendations | Supporting Information

ABSTRACT: Dry eye disease is becoming increasingly prevalent, and lubricating eye drops, a mainstay of its treatment, have a short duration of time on the ocular surface. Although there are various drug delivery methods to increase the ocular surface residence time of a topical lubricant, the main problem is the burst release from these delivery systems. To overcome this limitation, herein, a chemical−physical interpenetrating network (IPN) was fabricated to take control over the release of poly(vinyl alcohol) (PVA), a well-known therapeutic agent used to stabilize tear film, from gelatin methacrylate (GelMA) hydrogels. In this report, PVA was specifically used as part of a GelMA-based polymeric hydrogel owing to its physical cross-linking ability via a simple freeze-thaw method. The interpenetrating polymer network was fabricated in a sequential manner where GelMA was chemically cross-linked by photo-cross-linking, followed by physical cross-linking of PVA using a relatively short freeze-thaw cycle. Interestingly, upon applying only one short freeze-thaw cycle (of 1 or 2 h), the crystalline domains in PVA were increased in the interpenetrating network. The endothermic peaks at 48 and 60 °C in differential scanning calorimetry (DSC) thermograms and 20°−2θ peaks in X-ray diffraction (XRD) patterns suggest the presence of these crystalline domains. With the help of a suite of characterization, we further delineate the role of freeze-thaw cycles in taking control over the release of PVA. The release profiles of the PVA-containing hydrogels showed highest linearity with the Korsmeyer−Peppas model ($0.9944 < R^2 < 0.9952$), indicating that these systems follow non-Fickian or anomalous transport.

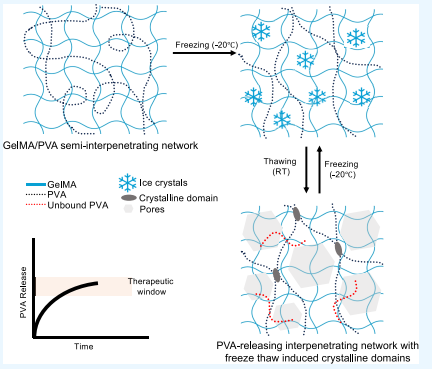

1. INTRODUCTION

The human eye is one of the most complex organs in the human body and can be divided into anterior (consisting of cornea, conjunctiva, aqueous humor, iris ciliary body, and crystalline lens) and posterior (consisting of sclera, choroid, and retinal pigment epithelium) segments.[1] Globally, a number of individuals are impacted by different ocular conditions, which directly compromise their vision and overall quality of life. Although eye drops have been used to administer about 90% of medications to the eye,[2] they have a low bioavailability due to dilution by the tears and rapid drainage from the ocular surface.[3] As a result, the development of long-lasting ophthalmic formulations for a wide variety of eye diseases is of great interest to both researchers and eye care practitioners. Soft, hydrophilic contact lenses have often been discussed as a potential option to deliver drugs to the ocular surface.[4,5] One potential application of soft hydrogels is in the treatment of dry eye,[6] a common ocular surface disorder that affects a substantial segment of the population.[7,8]

Hydrogels are three-dimensional, highly hydrophilic, soft polymeric materials that are used in a broad range of biomedical applications, including contact lenses,[9] and *in vitro* and *in vivo* as drug delivery platforms.[10,11] Hydrogels are of great interest for ocular drug delivery as they can increase the therapeutic efficacy of ophthalmic drugs by increasing the drug residence time at the site of administration and can facilitate codelivery of multiple drugs.[12−14] Gelatin derivatives, in particular, gelatin methacrylate (GelMA) hydrogels, are attractive candidates for biomedical use due to their outstanding biocompatibility[15] and can easily form a 3D network via physical or chemical cross-linking.[16] The photo cross-linking method used to cross-link GelMA can be performed in mild cross-linking conditions (room temperature, neutral pH, in aqueous environments, etc.), with a short reaction time and low cytotoxicity.[15,17] GelMA materials are highly biocompatible and versatile and can be used for a variety of ocular applications such as their use as bioinks for fabricating biodegradable drug delivery systems,[18] sustained drug release systems to be potentially used as ocular inserts,[19] injectable hydrogels for delivery of ocular drugs,[20] MMP-triggered controlled release vehicle for hyaluronic acid and model drugs for the potential treatment of corneal epithelial wound healing,[21] cell-loaded interpenetrating hydrogel networks as corneal stroma substitutes,[22] controlled release of vitamins for

Received: September 27, 2024
Revised: November 25, 2024
Accepted: December 16, 2024
Published: December 21, 2024

the treatment of the ocular surface, corneal healing, and acceleration of epithelial growth, while concurrently preventing potential inflammation.[23] Gelatin backbone could also be grafted with simple chemical modifications with glycidyl methacrylate to obtain an elastic protein-based hydrogel with biomimetic properties. Such properties allow to tune their viscoelastic and mechanical properties to facilitate their ocular applications.[24] Moreover, to understand the process of mass transport of a therapeutic agent through a hydrogel, it is important to gain insights into its macroscopic properties, such as porosity and cross-link density. Increasing the composition of the polymer phase in a hydrogel network and therefore the cross-link density is one strategy to modulate the drug release from GelMA hydrogels.[25] One method to potentially increase the cross-link density of GelMA could be obtained by forming GelMA-based interpenetrating networks.

Interpenetrating polymer networks are made up of two or more distinct polymer networks, where the macromolecular chains of each network permeate through one another without being covalently bound to each other. Compared to hydrogels with a single network, interpenetrating networks have a partial interlacing on the molecular scale and are reported to provide improved mechanical and dynamic properties.[26−28] Poly(vinyl alcohol) (PVA) is a commonly used viscosity enhancer in eye drops[29] with the capability of reducing symptoms of dry eye by stabilizing the tear film and reducing evaporation.[30] It can be cross-linked using physical methods such as freeze-thaw cycles without the addition of reactive chemicals, which is inherently more biocompatible.[31]

PVA hydrogels have been used for fabricating drug delivery systems for wound healing;[32] as antibacterial agents,[33,34] anti-inflammatory agents,[35] and anticancer agents;[36] and for targeted release.[37] It is anticipated that a GelMA−PVA interpenetrating network would display properties of both polymers and demonstrate enhanced biocompatibility and mechanical properties.[38] Upon freeze thawing of PVA, the crystalline domain formation is increased, and this concept could potentially be used as a strategy to modify the release rate of therapeutic molecules from drug delivery platforms.[39,40]

The release profiles of PVA from commercially available hydrogel contact lens materials exhibit rapid initial release.[41,42] To overcome this limitation, we report a PVA-releasing interpenetrating network of GelMA and PVA fabricated in a sequential manner (chemical−physical double network) for therapeutically promising outcomes. In the first step, GelMA part is photo cross-linked. In the second step, ice crystal formation occurs during the freezing cycle and subsequent thawing leads to the formation of hydrogen bonds between the PVA chains, creating "physical cross-links" without the need for any additional chemical cross-linkers. In this study, relatively short freeze-thaw (FT) cycles were applied to physically cross-link PVA and precisely tune crystallization, hydrogen bonding, and final network properties to take control over the rate of PVA release by leveraging its physical cross-linking abilities.

2. MATERIALS AND METHODS

2.1. Synthesis of GelMA. GelMA was prepared by direct reaction of type A gelatin (40 g, 300 Bloom, Sigma, St. Louis, Missouri, USA) with methacrylic anhydride (1% v/v, Sigma, St. Louis, Missouri, USA) in carbonate bicarbonate buffer (12.5 mM sodium bicarbonate, 87.5 mM sodium carbonate anhydrous, pH 9.4, 400 mL) buffer at 50 °C for 1 h. The substitution reaction was stopped by adding acetic acid (6 mL, 10%), and the resulting product was dialyzed in 12−14 kDa dialysis tubes (Sigma, St. Louis, Missouri, USA) in deionized water for 24 h to remove low molecular weight impurities. After dialysis, the GelMA solution was freeze-dried and stored at −80 °C until further use.[43]

2.2. Preparation of GelMA and GelMA/PVA Hydrogel Discs. To prepare the GelMA prepolymer solution, GelMA (10% w/v) was added to lithium phenyl-2,4,6-trimethylbenzoylphosphinate (0.6% w/v, LAP, Sigma, St. Louis, Missouri, USA) solution made in phosphate-buffered saline (PBS, Fisher Scientific, Waltham, Massachusetts, USA). To make PVA/GelMA (P-Gel) prepolymer solution, GelMA (20% w/v) was added to a LAP solution dissolved in PBS (1.2% w/v). PVA (10% w/v, molecular weight 89−98 kDa, 99+% hydrolyzed, Sigma, St. Louis, Missouri, USA) solution was made separately in PBS and heated to 90 °C until completely dissolved. The two solutions were added in a 1:1 ratio to make the P-Gel prepolymer solution comprising GelMA (10%), PVA (5%), and LAP (0.6%). These solutions were incubated at 37 °C for 1 h before use. The GelMA and P-Gel prepolymer solutions were photopolymerized by using a UV lamp fitted into a custom-made box (wavelength 405 nm, 60 W output, and 10 cm distance from the light source) to fabricate discs of 10 mm in diameter and 4 mm in thickness. The discs were cross-linked for 2 min on both sides to ensure complete cross-linking. The P-Gel hydrogel discs then underwent a single freeze-thaw cycle at −20 °C for 1 h (P-Gel-1FT) and 2 h (P-Gel-2FT).[44]

2.3. Morphological Characterization. To gain insights into the hydrogels, the samples were first swollen in PBS (pH 7.4), followed by freezing at −80 °C overnight and then freeze-drying (Labconco Freeze-Dry System FreeZone 2.5 Liter, 7670000, Kansas City, Missouri, USA) for 24 h. The freeze-dried samples were fixed on an aluminum stub by using double-sided adhesive conducting carbon tape and then imaged using environmental scanning electron microscopy (ESEM, Quanta FEG 250, FEI Company, Hillsboro, Oregon, USA). The SEM images were used to calculate the pore sizes using ImageJ software, and the pore size distributions were plotted in OriginPro 2024 software.

2.4. Chemical Characterization. Fourier transform infrared (FTIR) measurements were made with a Bruker Tensor 27 (Karlsruhe, Germany) in attenuated reflectance mode (ATR, PIKE Technologies, Fitchburg, Wisconsin, USA) between 600 and 4000 cm^{-1} at a fixed resolution of 4 cm^{-1}. Nuclear magnetic resonance (NMR) spectra were obtained using a Bruker Ascend 300 MHz spectrometer using D_2O as solvent at 14 mg/mL at room temperature. Powder X-ray diffraction (XRD) patterns for the samples were recorded in the 2θ range 10−50° using a Cu Kα radiation Bruker D8 (Karlsruhe, Germany).

2.5. Thermal Analysis. Differential scanning calorimetry (DSC) analysis was carried out using a Q 2000 (TA Instruments, New Castle, Delaware, USA). The sample (8 to 12 mg) was taken and weighed in an aluminum pan with a lid and underwent cyclic DSC of heating cycles of 10 °C/min up to 200 °C in the first cycle and a cooling cycle of 10 °C/min under nitrogen purge (50 mL/min). In the second heating cycle, the sample was heated from 25 to 250 °C. The data from the two heating cycles were recorded for analysis.

2.6. Swelling Behavior. Swelling ratios of the hydrogels were measured by using a gravimetric method. The hydrogel discs were freeze-dried initially, and their weights were noted.

https://doi.org/10.1021/acsomega.4c08667
ACS Omega 2025, 10, 1249−1260

Table 1. Curve Fitting of Various Models for Drug Release Kinetics

	zero order	first order	Higuchi model	Korsmeyer–Peppas model
equation	$C_t = C_o + K_o t$	$\log C_t = \log C_o - (K_1/2.303)t$	$M_t/M_\infty = K_h t^{1/2}$	$\log(M_t/M_\infty) = \log K_{kp} + n \log t$
graph	cumulative drug release vs time	log cumulative % drug remaining vs time	cumulative % drug release vs $\sqrt{t}$	log(cumulative % drug release) vs log t

These discs were incubated in 4 mL of PBS at 35 °C and 50 rpm and allowed to swell for 24 h. At fixed time intervals, the samples were removed from PBS; the surface water was soaked gently, and the weight at time t was noted until equilibrium swelling was reached. At any given time, t, the swelling ratio was calculated using the following equation:

$$\text{swelling ratio} = (W_t - W_i)/W_i \times 100$$

where W_i represents the initial dry weight of the hydrogels, whereas W_t is defined as the weight of the swollen hydrogels at time t. The swelling kinetics were studied using the power law, and a graph was plotted between $\log(M_t/M_\infty)$ versus $\log t$ with the help of GraphPad Prism. Here, M_t represents the weight of hydrogel at time t and M_∞ represents the weight at equilibrium swelling. Slope of the curves were calculated to determine the diffusional exponent n.

2.7. Mechanical Properties. Hydrogel samples (12 mm height and 10 mm diameter) were swollen for 24 h at room temperature in a PBS buffer at pH 7.4 prior to mechanical measurements. The compression tests were performed on a Texture Analyzer (Hamilton, Massachusetts, USA) universal testing machine (UTM) model XTPlus using Texture Exponent software. The swollen hydrogel samples were dabbed gently with tissue paper to discard surface water prior to the compressive test. Each sample was positioned in the middle of the stage, and the load cell of 5 kg was used.

2.8. Release and Detection of PVA. The P-Gel, P-Gel-1FT, and P-Gel-2FT hydrogel discs were incubated in glass vials with 10 mL of PBS solution at 35 °C and 50 rpm. At each indicated time point, 300 μL of the solution was removed for detection of PVA and replaced with fresh PBS. For detection of PVA, the method reported by Procházková et al. was used with slight modifications. Briefly, a solution of iodine (150 mM potassium iodide, 50 mM diiodine in deionized water, Sigma 221945 and 207772, St. Louis, Missouri, USA) was mixed with borate (64.7 mM boric acid in deionized water, Sigma B0394, St. Louis, Missouri, USA) in a 1:5 ratio of iodine solution:borate solution to generate the PVA detection solution. The solution was gently inverted four to six times in a conical tube to ensure even mixing. To measure PVA in solution, 163.6 μL of PVA detection solution was added to 36.4 μL of samples of interest in a 96-well plate and incubated at room temperature for 20 min with gentle shaking. Absorbances were read at 630 nm using an Imaging Multimode Plate Reader (Cytation 5, Agilent BioTek Instruments, Winooski, Vermont, USA).[45]

2.9. Drug Release Kinetics via Mathematical Modeling. To evaluate release kinetic profiles of the samples over the studied time duration, different mathematical models were studied.[46] These included the zero- and first-order release model, Higuchi release model, and Korsmeyer–Peppas model (Supporting Information). The graphs were plotted as mentioned in Table 1, and the coefficient of determination (R^2) was calculated for each model.[47,48]

2.10. Cytotoxicity Evaluation. The 3-[4,5-dimethylthiazol-2-yl]-2,5-diphenyltetrazolium bromide (MTT) assay was conducted to assess the cytotoxicity of the GelMA and P-Gel hydrogels with HCECs (human corneal epithelial cells). HCECs were routinely cultured in DMEM/F12 medium (Sigma, St. Louis, Missouri, USA) containing 1% FBS and 1% penicillin/streptomycin (Thermo Fisher Scientific, Waltham, Massachusetts, USA) at 37 °C and 5% CO_2 in a humidified atmosphere.

For the MTT assay, the cells were seeded in a 96-well plate at a density of 1×10^4 cells per well using complete culture medium. The hydrogel discs (weighing about 10 mg) were sterilized by exposing them to ultraviolet light for 30 min before incubation with the cells. A sterilized solution of 0.2% (w/v) PVA was made in culture media, and a 200 μL sample was used for the cytocompatibility assay. After incubating the sterilized hydrogels and PVA solutions with cells for 24 h, the cells were washed with PBS and treated with 1 mg/mL MTT solution prepared in culture media. The MTT solution was removed after 4 h of incubation, 150 μL of DMSO was added to each well to dissolve the formazan crystals, and the absorbance was measured at 570 nm using a microplate reader (Cytation 5, Agilent BioTek Instruments, Winooski, Vermont, USA). All conditions were taken in triplicates. The viability of HCEC cells was calculated according to the following formula.[49]

$$\text{cell viability}(\%) = \frac{\text{absorbance of test} - \text{absorbance of blank}}{\text{absorbance of control} - \text{absorbance of blank}} \times 100$$

2.11. Statistical Analysis. Statistical analysis was performed using GraphPad Prism 10.1.2 (GraphPad Software, La Jolla, California, USA). All data are reported as mean and standard deviation, unless otherwise stated. Two-way ANOVA was performed to determine differences across testing groups. Tukey's multiple comparison tests were used when necessary. In all cases, statistical significance was considered significant for a p value of <0.05 unless otherwise stated.

3. RESULTS AND DISCUSSION

3.1. Morphological Characterization. SEM images of all of the hydrogels displayed a highly interconnected porous architecture (Figure 1a–d). GelMA hydrogels had a very broad pore size distribution, with pore sizes ranging from 1 to 90 μm and mean pore size of 23 μm (Figure 2a). The pore size distribution for P-Gel samples was in the range of 1 to 60 μm with a mean pore size of 18 μm (Figure 2b). The pore size distribution of freeze-thawed P-Gel hydrogels (Figure 2c,d) was observed to be similar to P-Gel samples, where the pore sizes decreased and were more uniform compared to the GelMA sample. It is interesting to note a remarkably narrower pore size distribution upon addition of PVA. This smaller and more homogeneous pore architecture along with slightly thicker pore walls suggests a good compatibility between GelMA and PVA.[50,51]

The morphology of the P-Gel hydrogels in Figure 1b could be attributed to formation of a semi-interpenetrating network, where GelMA forms a chemically cross-linked network

https://doi.org/10.1021/acsomega.4c08667
ACS Omega 2025, 10, 1249–1260

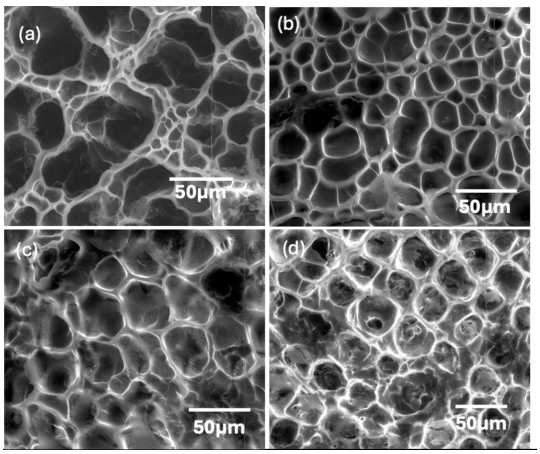

Figure 1. Cross-sectional SEM images of the freeze-dried (a) GelMA, (b) P-Gel, (c) P-Gel-1FT, and (d) P-Gel-2FT hydrogels showing a highly interconnected porous structure. The pore architecture becomes more uniform with the addition of PVA.

through photo-cross-linking. During the freezing step in the lyophilization process, thermally induced phase separation occurs between the solvent phase and the polymer phase, creating a polymeric network.[52] The larger pore size of GelMA hydrogels (Figure 1a) could be attributed to the presence of a less polymeric phase in GelMA hydrogels (10% GelMA) compared to the P-Gel samples (10% GelMA and 5% PVA). Thus, GelMA hydrogels hold more water to undergo ice crystal formation during the freezing step, leading to relatively larger pore sizes (Figure 1a). Moreover, PVA molecules might penetrate and partially fill the free voids between GelMA chains, thus increasing the cross-linking density and resulting in the formation of smaller-sized pores between the cross-linked GelMA chains (Figure 1b–d).[53]

3.2. Chemical Characterization. *3.2.1. FTIR Spectroscopy.* When gelatin is reacted with methacrylic anhydride, gelatin undergoes amidation to form GelMA. During the reaction, nucleophilic attack of a primary amine to the carbonyl carbon of methacrylic anhydride takes place, where an amide linkage is formed following amine deprotonation. In the next step, the photoinitiator initiates free radical polymerization upon

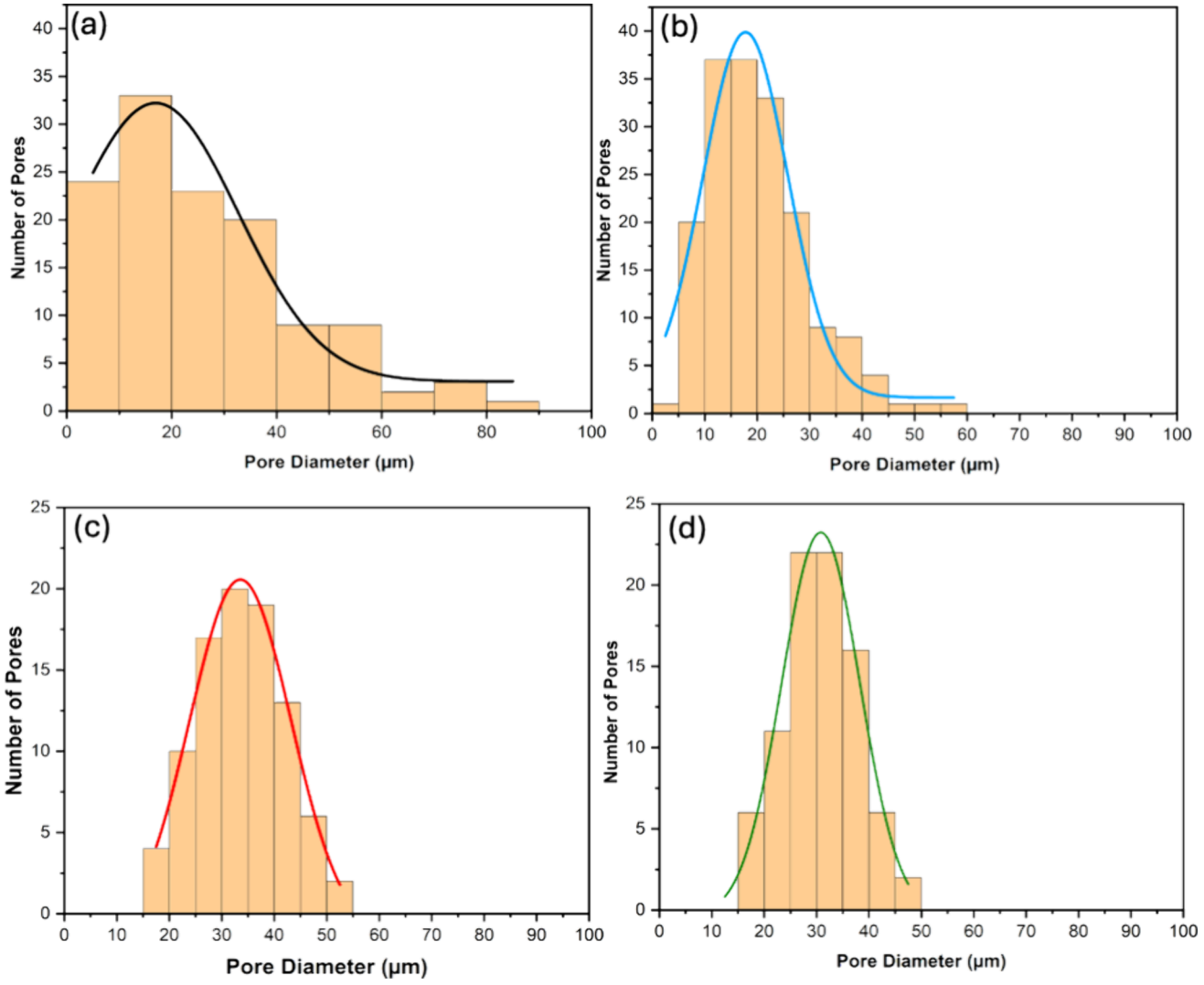

Figure 2. Pore size distribution of (a) GelMA, (b) P-Gel, (c) P-Gel-1FT, and (d) P-Gel-2FT. GelMA shows a broad pore size distribution with pore sizes ranging from 1 to 90 μm, with most pores ranging from 15 to 20 μm. The P-Gel samples showed more uniform pore sizes with mean pore sizes of 10–25 μm.

https://doi.org/10.1021/acsomega.4c08667
ACS Omega 2025, 10, 1249–1260

exposure to UV light (405 nm) and forms cross-linked GelMA hydrogels. Multiple peaks between ~3500 and 3200 cm^{-1} resemble the O−H stretching and N−H stretching, whereas the peak at ~2936 cm^{-1} is attributed to the C−H stretching.[54] The peak at ~1640 cm^{-1} in GelMA represents the C═O stretching (amide I).[55] The peak around 1640 cm^{-1} corresponding to the C═C stretching of the methacrylate groups is close to the C═O stretching peak of amide I, making it difficult to verify its disappearance after the cross-linking process in the GelMA spectrum.[56] The peak at ~1534 cm^{-1} corresponds to N−H bending and stretching vibrations of C−N groups (amide II), and the peaks around ~1445 and ~1335 cm^{-1} are assigned to $-CH_2$ bending vibrations and C−N stretching vibrations within amide III, respectively.[57−59] In the PVA FTIR spectrum, the peak around ~1140 cm^{-1} corresponds to the C−O and C−C stretching, denoting its crystalline regions.[54,60] This band is observed in the P-Gel prepolymer solution and hydrogels, indicating the presence of PVA. The sharp peak at ~1092 cm^{-1} in the PVA spectrum corresponds to the C−O vibration.[58] When PVA is added to the GelMA polymer solution, it might undergo supramolecular interactions (H-bonding) between the $-OH/-NH_2$ groups of PVA and GelMA. The appearance of a shoulder around ~1088 cm^{-1} in the P-Gel hydrogel interactions may be attributed to these supramolecular interactions (Figure 3). These supramolecular interactions may also be the source of the additional transition that appeared at around 48 °C in the DSC thermograms of P-Gel-2FT in the first heating cycle (Figure 5b).

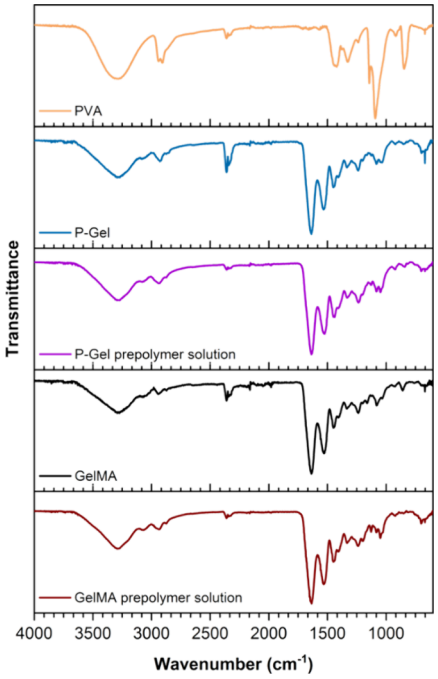

Figure 3. FTIR spectra of GelMA prepolymer solution, GelMA hydrogels, P-Gel prepolymer solution, P-Gel hydrogels, and PVA powder.

3.2.2. NMR. The GelMA macromers were functionalized using methacrylic anhydride (4.0 mL per 4 g of gelatin) during the reaction. The conjugation of methacryloyl groups to gelatin molecules was monitored and confirmed by ^{1}HNMR spectroscopy (Figure 4). Appearance of the signals at 5.36 and 5.62 ppm (the protons of the vinyl group of methacrylic anhydride) and decrease of the signal at 2.92 ppm (the protons of methylene of lysine signal) confirmed the modification of gelatin with methacrylic anhydride. Since the proton signal of the aromatic amino acid moieties in gelatin remained constant, the intensity of these protons was used to normalize the intensity of these protons in gelatin and the synthesized GelMA. Therefore, the degree of substitution (DS) of GelMA was calculated by comparing the proton signal at 2.9 ppm of the unmodified gelatin with that of GelMA. The DS of GelMA was calculated as about 61.8% in this study, which is in good agreement with those previously reported for GelMA prepared in a similar condition.[61,62]

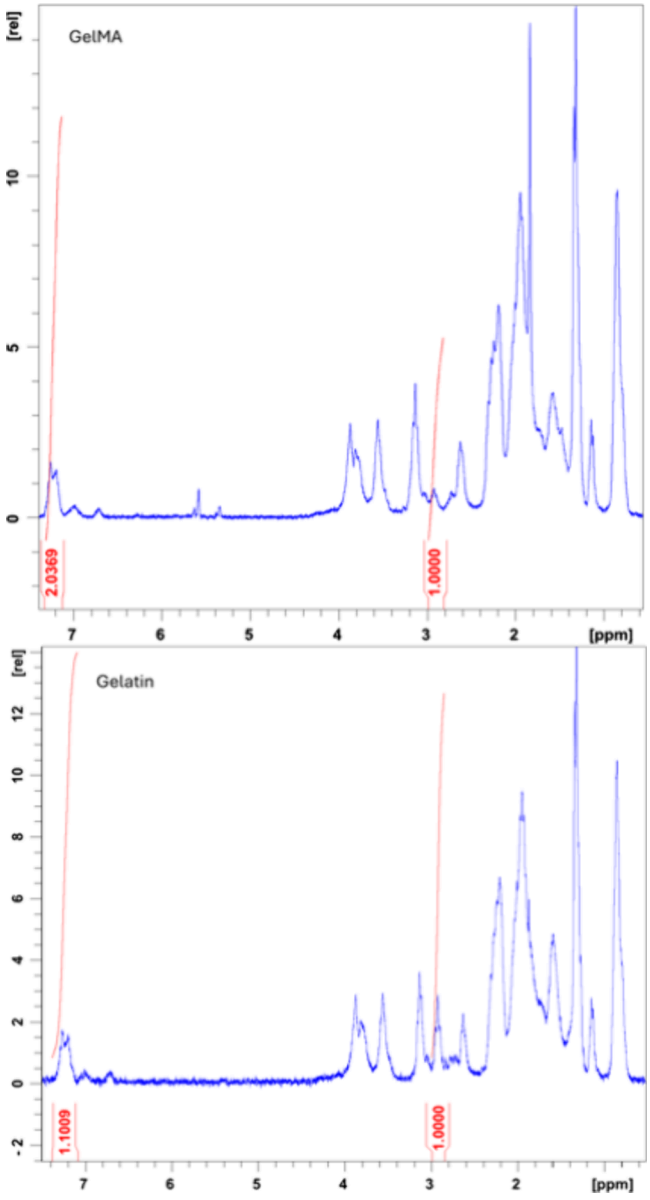

Figure 4. ^{1}HNMR spectra of gelatin and GelMA.

3.2.3. XRD. XRD patterns of the PVA powder and GelMA (Figure 5a) revealed that the PVA peak was around 22.5°−2θ, while that of GelMA was around 20°−2θ.[63] The peak around 20°−2θ and 41°−2θ in PVA represents the semicrystalline nature of PVA with both crystalline and amorphous regions.[64,65] XRD patterns of the P-Gel, P-Gel-1FT, and P-

https://doi.org/10.1021/acsomega.4c08667
ACS Omega 2025, 10, 1249−1260

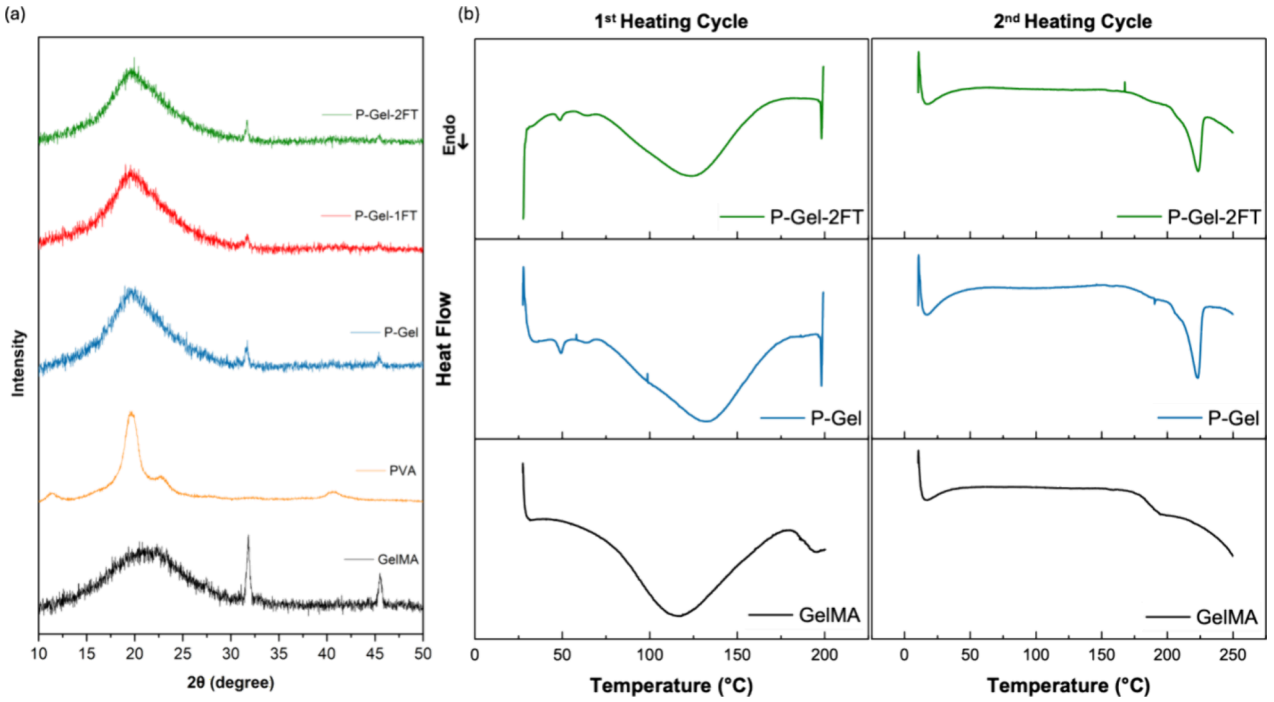

Figure 5. (a) XRD patterns of GelMA, PVA, P-Gel, P-Gel-1FT, and P-Gel-2FT samples. (b) DSC thermograms of GelMA, P-Gel, and P-Gel-2FT samples for the first (~200 °C) and second heating (~250 °C) cycle.

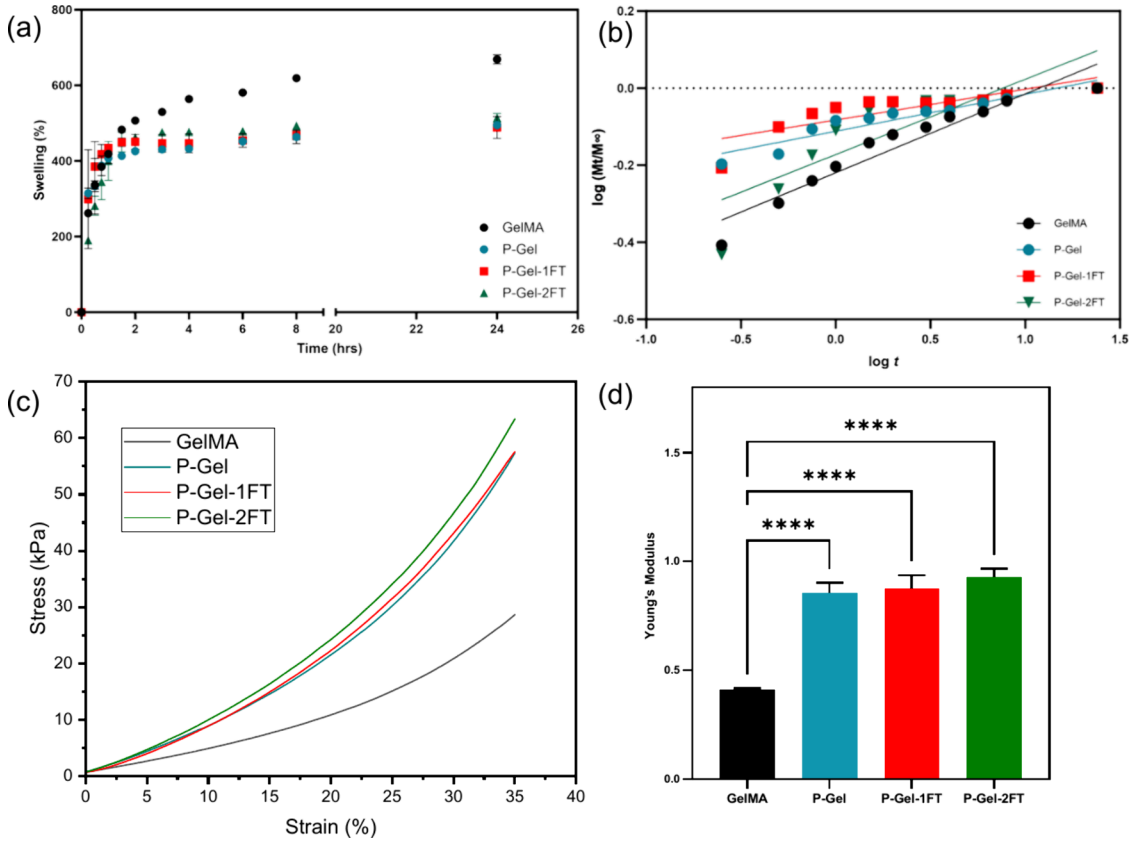

Figure 6. (a) Equilibrium swelling of GelMA, P-Gel, and freeze-thawed hydrogels. (b) Swelling kinetics analysis based on power law. (c) Stress–strain curves and (d) Young's modulus for GelMA, P-Gel, and freeze-thawed hydrogels.

Gel-2FT showed a prominent peak around 20°−2θ. From the GelMA XRD pattern, it is observed that the peak around 20°−2θ was broad; however, the PVA peak at 20°−2θ is relatively sharper and of higher intensity.[65] In the presence of PVA in the P-Gel-interpenetrating network, the diffraction pattern shows slight changes. The P-Gel hydrogel possesses a diffraction peak

https://doi.org/10.1021/acsomega.4c08667
ACS Omega 2025, 10, 1249−1260

at 20°−2θ, which is higher, and sharper compared to the diffraction pattern of GelMA. These results suggest that the hydrogen bond intermolecular interactions occur between the PVA and GelMA chains.[66] Similarly, in P-Gel-1FT and P-Gel-2FT samples, the 20°−2θ peak is relatively sharper and higher in intensity, indicating that crystallinity of the interpenetrating network could be mainly due to PVA.[67]

3.3. Thermal Analysis. Next, a thermal analysis was used to study the microstructure of the hydrogels. The first heating cycle in the DSC thermogram (Figure 5b) indicated broad endothermal transitions at around 113 °C for GelMA and 123 °C for P-Gel and P-Gel-2FT that correspond to evaporation of water molecules from the samples. During the second heating cycle, no exothermic or endothermal transition was observed in the GelMA sample, indicating that no further physical/chemical changes took place in this temperature range. Meanwhile, for P-Gel and P-Gel-2FT samples, two endothermal transitions were observed at around 48 and 62 °C in the first heating curve. Similar transitions have been previously reported for freeze-thawed PVA hydrogels at similar temperatures around 60 °C and are attributed to a gel-to-sol transition owing to dissociation of H-bonding and melting of the crystalline phase.[52] The transition around 48 °C in P-Gel and P-Gel-2FT hydrogels could be attributed to the supramolecular interactions (H-bonding) between the −OH/−NH_2 groups of PVA and GelMA and its effect on crystalline domain formation in PVA. The stability (melting temperature) and size (melting enthalpy) of the crystalline domains control mechanical and physical properties of the PVA-containing hydrogels, and these two parameters are influenced by the duration and number of freeze-thaw cycles.[68] The melting enthalpies of the P-Gel and P-Gel 2FT hydrogels were measured using the TA Universal Analysis 2000 v4.5A. An increase in enthalpy of the melting transition from P-Gel to P-Gel-2FT (0.3304 to 0.4104 J/g) in the temperature range of 48−60 °C supports increased crystallinity upon FT cycles and is in line with the literature reports.[68] As the temperature increased to 250 °C in the second heating cycle, an endothermal transition was observed in the P-Gel-2FT thermogram at around 225 °C, which corresponds to the melting of PVA in the samples.[69]

3.4. Swelling Behavior. The swelling behavior of the freeze-dried GelMA, P-Gel, P-Gel-1FT, and P-Gel-2FT hydrogels is shown in Figure 6a. A post hoc Tukey test was applied to identify any significant difference between the swelling behavior of the hydrogel samples. After 1.5 h, the GelMA hydrogel showed a significant difference in the swelling compared to the P-Gel sample ($p < 0.05$). From the swelling curves (Figure 6a), it can be inferred that P-Gel, P-Gel-1FT, and P-Gel-2FT samples undergo less swelling compared to GelMA. This reduced swelling could help to control the release and support a sustained release of PVA from the interpenetrating network. Moreover, there is a gradual decrease in the degree of swelling with increase in cross-link density owing to the presence of a lower polymeric phase in GelMA hydrogels compared to the P-Gel samples. This is also corroborated by the SEM results (Figure 1). Next, $\log(M_t/M_\infty)$ versus $\log t$ was plotted to understand the swelling kinetics (Figure 6b) of the hydrogels. Interestingly, the GelMA hydrogel showed the highest linearity (R^2 value = 0.9159) with the power law, indicating that the swelling of these gels followed Fickian diffusion (n value <0.45). Additionally, P-Gels, P-Gel-1FT, and P-Gel-2FT showed slightly smaller R^2 values (0.8884, 0.6764, and 0.7206, respectively). n values for these hydrogels were also found to be <0.45, indicating diffusion-controlled swelling.[70]

3.5. Mechanical Properties. Figure 6c shows the compressive stress−strain curves of the GelMA, P-Gel, P-Gel-1FT, and P-Gel-2FT hydrogels. The compression experiments suggest that the double networks containing PVA had a twofold higher compressive modulus (0.8564 ± 0.0457) than 10% GelMA alone (0.4099 ± 0.00829). The P-Gel hydrogels that underwent 1 and 2 h freeze thawing also exhibit a remarkable compressive modulus (Tables 2 and 3). This could

Table 2. Young's Modulus

Young's modulus (kPa)	GelMA	P-Gel	P-Gel-1FT	P-Gel-2FT
mean	0.4099	0.8564	0.8766	0.9302
SD	0.0082	0.0457	0.0596	0.0364

Table 3. Compressive Strength

stress (kPa)	GelMA	P-Gel	P-Gel-1FT	P-Gel-2FT
mean	26.4391	59.0745	62.7813	63.0322
SD	0.4161	1.5958	4.4641	0.7766

be attributed to the freeze thaw and solvent displacement process, which results in intensified physical interactions to form a second stiffer and tougher network of PVA.[38] These stronger noncovalent interactions could be the reason for a slight increase in the Young's modulus observed with the 1 and 2 h freeze-thawed samples (0.8766 ± 0.0596 and 0.9302 ± 0.0364, respectively, Figure 6d). Reports suggest that there are different gelation parameters (such as the number, temperature, and time of FT cycles) and polymer parameters (such as molecular weight, concentration, and degree of hydrolysis of PVA) that affect the final mechanical properties of PVA hydrogels.[52] Similarly, the mechanical properties of GelMA-based hydrogels are influenced by various parameters such as concentration and DS of GelMA, type and concentration of photoinitiator used, and intensity and duration of UV exposure.[71]

3.6. Release of PVA. PVA release curves (Figure 7) depict the effect of the freeze-thaw method in tuning the release of PVA. Interestingly, after the samples experienced a freeze-thaw

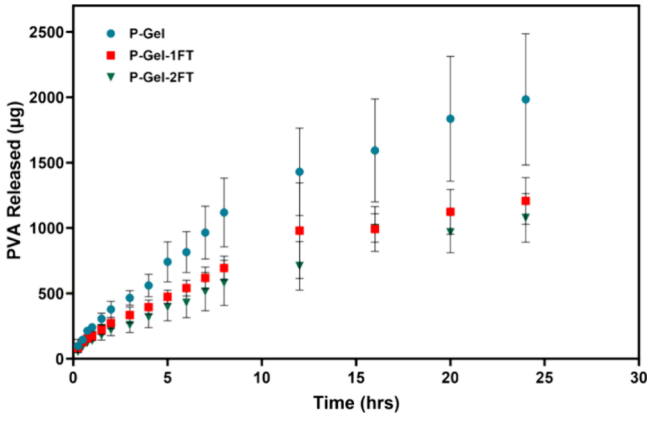

Figure 7. PVA release curves and the effect of freezing times on the release rate of PVA (per 100 mg hydrogel). The freeze-thawed samples show a lower release of PVA than the P-Gel samples, supporting the concept of using freeze-thaw cycles to control release rates.

https://doi.org/10.1021/acsomega.4c08667
ACS Omega 2025, 10, 1249−1260

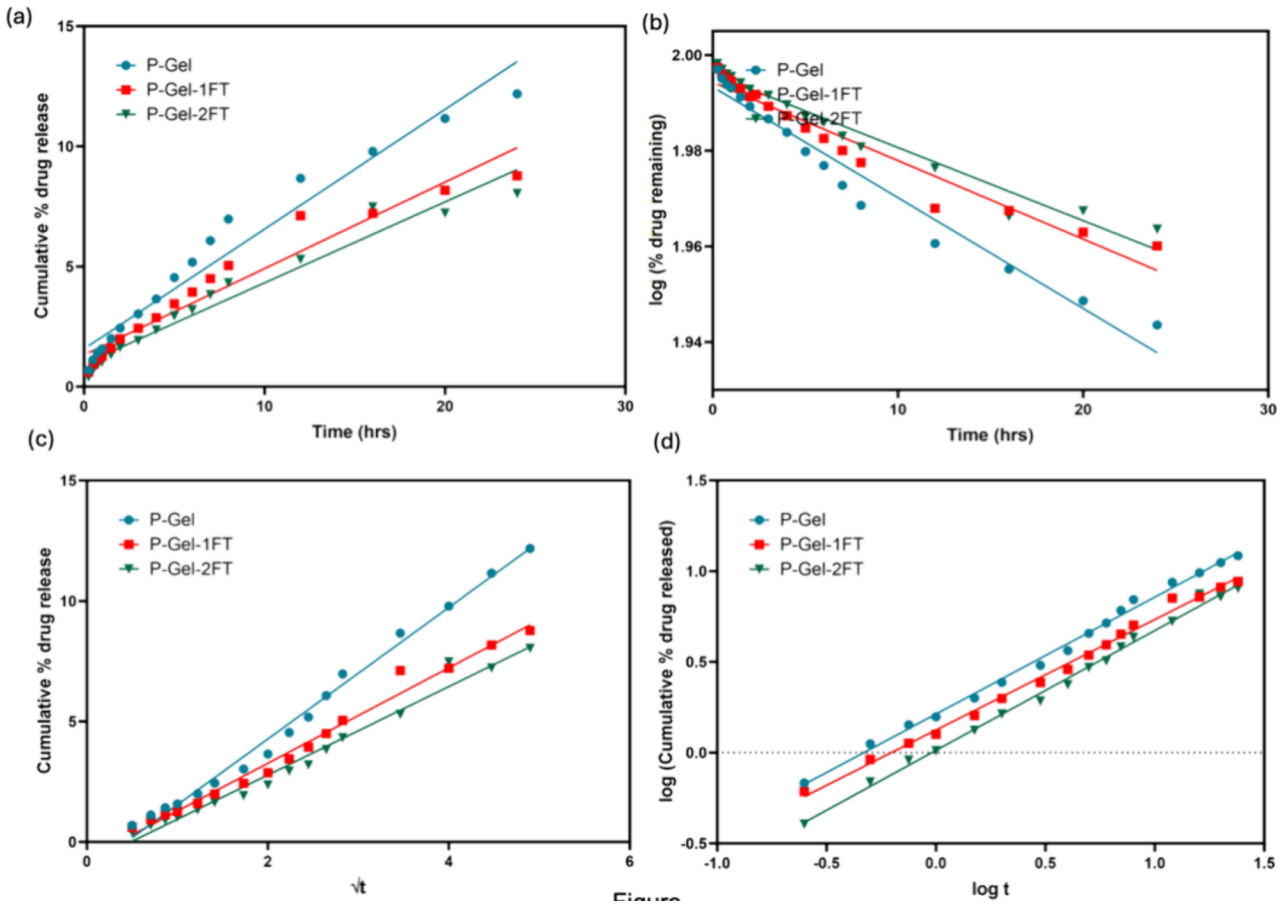

Figure 8. Modeling of the PVA release data on well-known mathematical models: (a) zero-order, (b) first-order, (c) Higuchi's model, and (d) Korsmeyer-Peppas model.

cycle of about 2 h, there was a lower release of PVA compared to P-Gel. A post hoc Tukey test was employed, which revealed that after 5 h, the P-Gel-2FT hydrogel exhibited significantly lower PVA release ($p < 0.05$) compared to P-Gels. Furthermore, the P-Gel-1FT sample showed significantly lower release of PVA after 7 h ($p < 0.05$) compared to P-Gels. The observed decrease in release of PVA by altering the freeze-thaw parameters is in good agreement with the concept of using freeze thaw to adjust the release rates of PVA. Although release of PVA from P-Gel-2FT is less than P-Gel-1FT samples (Figure 7), the difference was not statistically significant ($p > 0.0\ 5$).

There are three main processes that explain the effect of freeze-thaw cycles on the P-Gel semi-interpenetrating network; (a) hydrogen bonding, (b) crystalline domain formation, and (c) phase separation. During the freezing step, ice crystals are formed, which allow PVA chains to come closer and form PVA-rich domains.[52] The close proximity between these PVA chains promotes the formation of crystalline domains through inter- and intramolecular H-bonds that act as cross-linking sites. Upon thawing, these ice crystals melt, leaving behind pores surrounded by a PVA skeleton.[52] During successive freeze-thaw cycles, more PVA chains come into closer contact with each other and new crystalline domains or sites are generated. Theoretically, higher freezing durations cause more H-bonding to occur, increasing crystallinity.[52] Of note, it is important to consider the temperatures at which these hydrogels will be stored or used, because temperatures >60 °C could lead to gel-to-sol transition owing to dissociation of H-bonding and melting of the crystalline phase.[52] In our case, the desired application of these PVA-containing hydrogels would be to release this therapeutic agent on the ocular surface, which has a temperature of about 35 °C. There are various factors that influence crystallinity and water uptake of PVA-containing hydrogels, such as concentration of PVA, number of freeze-thaw cycles, molecular weight of PVA, temperature, and duration of freeze-thaw cycles,[52] suggesting that carefully designing these parameters for freeze-thaw cycles can help achieve tunable release rates.

3.7. Drug Release Kinetics via Mathematical Modeling. To study the drug release kinetics and how different factors affect the dissolution velocity and behaviors, various mathematical equations describing the release dependence on time are used. In this study, drug release was evaluated though four main release kinetic models: zero- (Figure 8a) and a first-order release model (Figure 8b), a Higuchi release model (Figure 8c), and a Korsmeyer−Peppas model (Figure 8d). In the context of drug release, zero-order release kinetics implies that the drug is released at a constant rate over time regardless of its initial concentration. This can be desirable for certain medications, as it provides a constant and predictable therapeutic effect. The first-order release kinetics describes the rate of drug release as being directly proportional to the initial concentration of the drug. This means that as the concentration of the drug decreases, the rate of release also decreases. Higuchi's model is based on Fickian diffusion and is specifically derived for drugs dispersed in solid or semisolid matrices, typically without considering the effect of swelling or

https://doi.org/10.1021/acsomega.4c08667
ACS Omega 2025, 10, 1249−1260

dissolution of the matrix. According to this model, the graph between the concentration of the drug and square root of time would be a linear function.[72] Korsmeyer–Peppas is a semiempirical model that describes several release mechanisms, including Fickian diffusion, Case II transport, or a combination of both (anomalous transport).[73]

To evaluate the best-fit model for the release profiles in our study, the goodness of fit for each model or the coefficient of determination (R^2) was calculated using GraphPad Prism. The release profiles of the PVA-containing hydrogels showed highest linearity with the Korsmeyer–Peppas model ($0.9944 < R^2 < 0.9952$). The release exponent (n) for P-Gel, P-Gel-1FT, and P-Gel-2FT samples were 0.6442, 0.6090, and 0.6601, respectively, indicating that these systems follow non-Fickian or anomalous transport (Table 4). This mechanism is governed by rate of time-dependent solute diffusion and swelling of the polymer matrix ($0.45 < n < 0.89$ and $n \neq 0.5$).[74] Moreover, the formation of crystalline domains upon freeze thawing can hinder the mobility of polymeric chains,[52] thus slowing their rearrangement. This along with the diffusion process occurring simultaneously causes time-dependent anomalous effects, thus explaining a better fit to the Korsmeyer–Peppas model.[73]

Table 4. Coefficient of Determination (R^2) Values of P-Gel, P-Gel-1FT, and P-Gel-2FT Calculated for Different Kinetic Models

kinetic model	P-Gel	P-Gel-1FT	P-Gel-2FT
zero-order	0.9568	0.9407	0.9560
first-order	0.9629	0.9449	0.9588
Higuchi	0.9914	0.9863	0.9798
Korsmeyer–Peppas	0.9954	0.9944	0.9952
diffusion exponent (n value)[a]	0.6442	0.6090	0.6601

[a]Calculated by the linear regression of the Korsmeyer–Peppas equation of $\log(M_t/M_\infty)$ versus $\log t$.

3.9. Cytotoxicity Evaluation. Cytotoxicity of biomaterials is an essential aspect for ocular applications. The efficacy and safety of a drug delivery vehicle depend on its ability to deliver the therapeutic agent specifically to the ocular surface while exhibiting no cytotoxicity. To realize this, we first investigated and compared the cytotoxicity of GelMA, P-Gel, P-Gel-2FT, and 0.2% (w/v) PVA solution using the MTT assay. The cell viability in the presence of GelMA and P-Gel-5% samples were about 86.5 and 85.1%, respectively, after 24 h of incubation, indicating they were not cytotoxic to the cells (Figure 9). Similarly, freeze-thaw cycles did not induce any adverse effects on the cells. Moreover, 0.2% (w/v) PVA showed >80% cell viability, suggesting its nontoxic nature. This concentration was selected based on the PVA concentration released per time point (Figure S1, Supporting Information). These findings support the use of these hydrogels as suitable vehicles for applications in the controlled drug release of PVA.

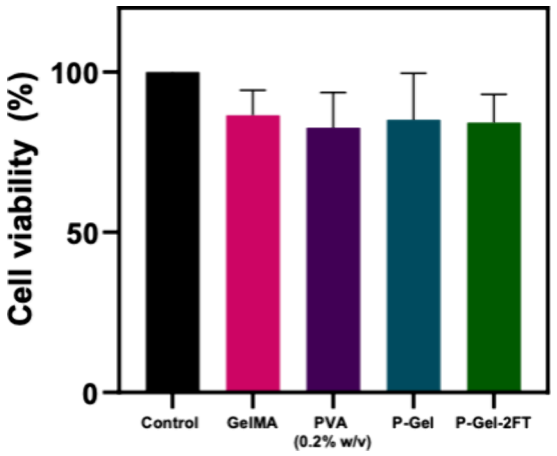

Figure 9. MTT assay for GelMA, PVA, P-Gel, and P-Gel-2FT.

4. CONCLUSIONS

In summary, the crystalline domains inside the PVA/GelMA chemical–physical interpenetrating network can be tuned to control the release rate of PVA, which is a commonly used therapeutic agent to treat dry eyes. The results from this study suggest that this method could potentially be easier to translate into application given the purported safety associated with utilizing a physical cross-linking method to create desired release profiles, as opposed to employing additional harsh chemical cross-linking agents. Of note, there are various factors such as concentration and molecular weight of PVA, number, temperature, and duration of freeze-thaw cycles that influence the physical and chemical properties of PVA-containing hydrogels, suggesting that engineering these parameters is crucial to taking control over the release rate of PVA. Furthermore, the macroscopic properties of these hydrogels are determined by the relative amount of crystalline and amorphous phases of PVA present. Looking ahead, we envisage that the physical barriers created with freeze-thaw cycles may also be explored to take control over the release of other molecules of interest from these gels. Interestingly, the versatile properties of GelMA could be explored to fabricate drug-eluting contact lenses or drug-loaded ocular inserts to be placed in cul-de-sac in the lower eyelid, providing prolonged release of molecules of interests.

■ ASSOCIATED CONTENT

Supporting Information

The Supporting Information is available free of charge at https://pubs.acs.org/doi/10.1021/acsomega.4c08667.

Drug release kinetics equations and PVA release per time points (PDF)

■ AUTHOR INFORMATION

Corresponding Author

Lyndon Jones − *Centre for Ocular Research & Education (CORE), School of Optometry & Vision Science, University of Waterloo, Waterloo N2L 3G1 ON, Canada; Centre for Eye and Vision Research (CEVR), Hong Kong 17W, Hong Kong*; Email: lwjones@uwaterloo.ca

Authors

Piyush Garg − *Centre for Ocular Research & Education (CORE), School of Optometry & Vision Science, University of Waterloo, Waterloo N2L 3G1 ON, Canada;* orcid.org/0000-0003-4544-4222

Parvin Shokrollahi − *Centre for Ocular Research & Education (CORE), School of Optometry & Vision Science, University of Waterloo, Waterloo N2L 3G1 ON, Canada; Centre for Eye and Vision Research (CEVR), Hong Kong 17W, Hong Kong*

https://doi.org/10.1021/acsomega.4c08667
ACS Omega 2025, 10, 1249−1260

Haile Fentahun Darge − *Centre for Ocular Research & Education (CORE), School of Optometry & Vision Science, University of Waterloo, Waterloo N2L 3G1 ON, Canada;* orcid.org/0000-0001-6022-0820

Chau-Minh Phan − *Centre for Ocular Research & Education (CORE), School of Optometry & Vision Science, University of Waterloo, Waterloo N2L 3G1 ON, Canada; Centre for Eye and Vision Research (CEVR), Hong Kong 17W, Hong Kong*

Complete contact information is available at: https://pubs.acs.org/10.1021/acsomega.4c08667

Notes

The authors declare the following competing financial interest(s): Over the past 3 years CORE has received research support or lectureship honoraria from Alcon, Azura Ophthalmics, Bausch Health, CooperVision, Essilor, Hoya, i-Med Pharma, Integral Biosystems, J&J Vision, Menicon, Novartis, Ophtecs, Ot Pharma, Santen, SightGlass, SightSage, Topcon and Visioneering. Lyndon Jones is also a consultant and/or serves on an advisory board for Alcon, CooperVision, J&J Vision, Novartis and Ophtecs.

■ ACKNOWLEDGMENTS

This project was supported and funded by Mitacs (through the Mitacs Accelerate program), the InnoHK initiative, the Hong Kong Special Administrative Region Government, the Canadian Optometric Trust Education Fund (COETF), and the Natural Sciences and Engineering Research Council of Canada's (NSERC) Collaborative Research and Training Experience (CREATE) program. The authors greatly appreciate the support provided by Dr Charles Dal Castel and Dr Faten Salim from Department of Chemical Engineering at the University of Waterloo during the material characterization. P.G. would also like to thank the University of Waterloo and Ontario Government for providing financial support in the form of fellowships and scholarships.

■ REFERENCES

(1) Seo, H.; Chung, W. G.; Kwon, Y. W.; Kim, S.; Hong, Y. M.; Park, W.; Kim, E.; Lee, J.; Lee, S.; Kim, M.; Lim, K.; Jeong, I.; Song, H.; Park, J. U. Smart Contact Lenses as Wearable Ophthalmic Devices for Disease Monitoring and Health Management. *Chem. Rev.* **2023**, *123* (19), 11488−11558.

(2) Lanier, O. L.; Manfre, M. G.; Bailey, C.; Liu, Z.; Sparks, Z.; Kulkarni, S.; Chauhan, A. Review of Approaches for Increasing Ophthalmic Bioavailability for Eye Drop Formulations. *AAPS PharmSciTech* **2021**, *22* (3), 107.

(3) Rykowska, I.; Nowak, I.; Nowak, R. Soft Contact Lenses as Drug Delivery Systems: A Review. *Molecules* **2021**, *26* (18), 5577.

(4) Maulvi, F. A.; Soni, T. G.; Shah, D. O. Extended release of hyaluronic acid from hydrogel contact lenses for dry eye syndrome. *Journal of Biomaterials Science, Polymer Edition* **2015**, *26* (15), 1035−1050.

(5) Li, R.; Guan, X.; Lin, X.; Guan, P.; Zhang, X.; Rao, Z.; Du, L.; Zhao, J.; Rong, J.; Zhao, J. Poly (2-hydroxyethyl methacrylate)/β-cyclodextrin-hyaluronan contact lens with tear protein adsorption resistance and sustained drug delivery for ophthalmic diseases. *Acta Biomaterialia* **2020**, *110*, 105−118.

(6) Yu, Y.; Chow, D. W. Y.; Lau, C. M. L.; Zhou, G.; Back, W.; Xu, J.; Carim, S.; Chau, Y. A bioinspired synthetic soft hydrogel for the treatment of dry eye. *Bioeng Transl Med.* **2021**, *6* (3), No. e10227.

(7) Dana, R.; Meunier, J.; Markowitz, J. T.; Joseph, C.; Siffel, C. Patient-reported burden of dry eye disease in the United States: results of an online cross-sectional survey. *American Journal of Ophthalmology* **2020**, *216*, 7−17.

(8) Stapleton, F.; Alves, M.; Bunya, V. Y.; Jalbert, I.; Lekhanont, K.; Malet, F.; Na, K. S.; Schaumberg, D.; Uchino, M.; Vehof, J.; et al. TFOS DEWS II Epidemiology Report. *Ocul Surf.* **2017**, *15* (3), 334−365.

(9) Nicolson, P. C.; Vogt, J. Soft contact lens polymers: an evolution. *Biomaterials* **2001**, *22* (24), 3273−3283.

(10) Ruskowitz, E. R.; DeForest, C. A. Photoresponsive biomaterials for targeted drug delivery and 4D cell culture. *Nat. Rev. Mater.* **2018**, *3* (2), 1−17.

(11) Ooi, H. W.; Hafeez, S.; Van Blitterswijk, C.; Moroni, L.; Baker, M. B. Hydrogels that listen to cells: a review of cell-responsive strategies in biomaterial design for tissue regeneration. *Materials Horizons* **2017**, *4* (6), 1020−1040.

(12) White, C. J.; DiPasquale, S. A.; Byrne, M. E. Controlled release of multiple therapeutics from silicone hydrogel contact lenses. *Optometry and Vision Science* **2016**, *93* (4), 377−386.

(13) DiPasquale, S. A.; Uricoli, B.; DiCerbo, M. C.; Brown, T. L.; Byrne, M. E. Controlled release of multiple therapeutics from silicone hydrogel contact lenses for post-cataract/post-refractive surgery and uveitis treatment. *Translational Vision Science & Technology* **2021**, *10* (14), 5−5.

(14) Fang, G.; Yang, X.; Wang, Q.; Zhang, A.; Tang, B. Hydrogels-based ophthalmic drug delivery systems for treatment of ocular diseases. *Mater. Sci. Eng. C Mater. Biol. Appl.* **2021**, *127*, No. 112212.

(15) Yue, K.; Trujillo-de Santiago, G.; Alvarez, M. M.; Tamayol, A.; Annabi, N.; Khademhosseini, A. Synthesis, properties, and biomedical applications of gelatin methacryloyl (GelMA) hydrogels. *Biomaterials* **2015**, *73*, 254−271.

(16) Zhao, L.; Qi, X.; Cai, T.; Fan, Z.; Wang, H.; Du, X. Gelatin hydrogel/contact lens composites as rutin delivery systems for promoting corneal wound healing. *Drug Deliv* **2021**, *28* (1), 1951−1961.

(17) Nguyen, A. K.; Goering, P. L.; Reipa, V.; Narayan, R. J. Toxicity and photosensitizing assessment of gelatin methacryloyl-based hydrogels photoinitiated with lithium phenyl-2, 4, 6-trimethylbenzoylphosphinate in human primary renal proximal tubule epithelial cells. *Biointerphases* **2019**, *14* (2), No. 021007.

(18) Park, B. C.; Kim, H. T.; Koh, J. W. New biodegradable drug delivery system for patients with dry eye. *Korean Journal of Ophthalmology: KJO* **2021**, *35* (6), 455.

(19) Li, S.; Zhao, X.; Wang, Q.; Yu, F.; Li, W.; Bai, Y.; Shen, X.; Du, X.; He, D.; Yuan, J. Mechanoresponsive Drug Loading System with Tunable Host−Guest Interactions for Ocular Disease Treatment. *ACS Biomaterials Science & Engineering* **2022**, *8* (11), 4850−4862.

(20) Shen, C.; Zhao, X.; Ren, Z.; Yang, B.; Wang, X.; Hu, A.; Hu, J. In situ formation of injectable gelatin methacryloyl (GelMA) hydrogels for effective intraocular delivery of triamcinolone acetonide. *International Journal of Molecular Sciences* **2023**, *24* (5), 4957.

(21) Tse, J. W.; Rizwan, M.; Rasmussen, J.; Jones, L.; Yim, E. K. F. Gelatin Methacrylate as an Enzyme-Controlled Release Vehicle of Hyaluronic Acid for the Treatment of Recurrent Corneal Erosion. *ACS Appl. Bio Mater.* **2020**, *3* (9), 6214−6223.

(22) Kilic Bektas, C.; Hasirci, V. Cell Loaded GelMA: HEMA IPN hydrogels for corneal stroma engineering. *J. Mater. Sci.: Mater. Med.* **2020**, *31*, 1−15.

(23) Ayran, M.; Goyuk, Y.; Tiryaki, A.; Ulag, S.; Koyuncu, A. C. C.; Turhan, S. A.; Gunduz, O. Light-Processed 3D Bioprinting of Symblepharon Rings Fortified with l-Ascorbic Acid for Ocular Tissue Engineering. *Macromol. Mater. Eng.* **2024**, 2400057.

(24) Sharifi, S.; Islam, M. M.; Sharifi, H.; Islam, R.; Koza, D.; Reyes-Ortega, F.; Alba-Molina, D.; Nilsson, P. H.; Dohlman, C. H.; Mollnes, T. E.; Chodosh, J.; Gonzalez-Andrades, M. Tuning gelatin-based hydrogel towards bioadhesive ocular tissue engineering applications. *Bioactive materials* **2021**, *6* (11), 3947−3961.

(25) Piao, Y.; You, H.; Xu, T.; Bei, H.-P.; Piwko, I. Z.; Kwan, Y. Y.; Zhao, X. Biomedical applications of gelatin methacryloyl hydrogels. *Engineered Regeneration* **2021**, *2*, 47−56.

(26) Yang, H.; Fustin, C. Design and Applications of Dynamic Hydrogels Based on Reversible C═ N Bonds. *Macromol. Chem. Phys.* **2023**, *224* (20), 2300211.
(27) Sperling, L. H.; Klempner, D.; Sperling, L. H.; Utracki, L. A.; Sperling, L. H.*Interpenetrating polymer networks: an overview*; ACS Publications 1994.
(28) Zhao, X.; Chen, X.; Yuk, H.; Lin, S.; Liu, X.; Parada, G. Soft materials by design: unconventional polymer networks give extreme properties. *Chem. Rev.* **2021**, *121* (8), 4309−4372.
(29) Leone, G.; Consumi, M.; Pepi, S.; Pardini, A.; Bonechi, C.; Tamasi, G.; Donati, A.; Rossi, C.; Magnani, A. Modified low molecular weight poly-vinyl alcohol as viscosity enhancer. *Materials Today Communications* **2019**, *21*, No. 100634.
(30) Chaudhari, P.; Birangal, S.; Mavlankar, N.; Pal, A.; Mallela, L. S.; Roy, S.; Kodoth, A. K.; Ghate, V.; Nampoothiri, M.; Lewis, S. A. Oil-free eye drops containing cyclosporine A/cyclodextrin/PVA supramolecular complex as a treatment modality for dry eye disease. *Carbohydr. Polym.* **2022**, *297*, No. 120007.
(31) Hassan, C. M.; Peppas, N. A. Structure and morphology of freeze/thawed PVA hydrogels. *Macromolecules* **2000**, *33* (7), 2472−2479.
(32) Suneetha, M.; Hemalatha, D.; Kim, H.; Rao, K. K.; Han, S. S. Vanillin/fungal-derived carboxy methyl chitosan/polyvinyl alcohol hydrogels prepared by freeze-thawing for wound dressing applications. *Int. J. Biol. Macromol.* **2024**, No. 130910.
(33) Waresindo, W. X.; Luthfianti, H. R.; Edikresnha, D.; Suciati, T.; Noor, F. A.; Khairurrijal, K. A freeze−thaw PVA hydrogel loaded with guava leaf extract: Physical and antibacterial properties. *RSC Adv.* **2021**, *11* (48), 30156−30171.
(34) Edikresnha, D.; Suciati, T.; Suprijadi; Khairurrijal, K. Freeze-thawed hydrogel loaded by Piper crocatum extract with in-vitro antibacterial and release tests. *J. Mater. Res. Technol.* **2021**, *15*, 17−36.
(35) Figueroa-Pizano, M.; Vélaz, I.; Peñas, F.; Zavala-Rivera, P.; Rosas-Durazo, A.; Maldonado-Arce, A.; Martínez-Barbosa, M. Effect of freeze-thawing conditions for preparation of chitosan-poly (vinyl alcohol) hydrogels and drug release studies. *Carbohydr. Polym.* **2018**, *195*, 476−485.
(36) Wu, Y.; Li, Y.; Han, R.; Long, Z.; Si, P.; Zhang, D. Dual-Cross-Linked PEI/PVA Hydrogel for pH-Responsive Drug Delivery. *Biomacromolecules* **2023**, *24* (11), 5364−5370.
(37) Ye, J.; Liu, L.; Lan, W.; Xiong, J. Targeted release of soybean peptide from CMC/PVA hydrogels in simulated intestinal fluid and their pharmacokinetics. *Carbohydr. Polym.* **2023**, *310*, No. 120713.
(38) Hu, Q.; Lu, R.; Liu, S.; Liu, Y.; Gu, Y.; Zhang, H. 3D printing GelMA/PVA interpenetrating polymer networks scaffolds mediated with CuO nanoparticles for angiogenesis. *Macromol. Biosci.* **2022**, *22* (10), 2200208.
(39) Bernal-Chávez, S. A.; Romero-Montero, A.; Hernández-Parra, H.; Peña-Corona, S. I.; Del Prado-Audelo, M. L.; Alcalá-Alcalá, S.; Cortés, H.; Kiyekbayeva, L.; Sharifi-Rad, J.; Leyva-Gómez, G. Enhancing chemical and physical stability of pharmaceuticals using freeze-thaw method: challenges and opportunities for process optimization through quality by design approach. *J. Biol. Eng.* **2023**, *17* (1), 35.
(40) Boran, F. The influence of freeze-thawing conditions on swelling and long-term stability properties of poly (vinyl alcohol) hydrogels for controlled drug release. *Polym. Bull.* **2021**, *78* (12), 7369−7387.
(41) Phan, C.-M.; Subbaraman, L. N.; Jones, L. W. Uptake and release of polyvinyl alcohol from hydrogel daily disposable contact lenses. *Optometry and Vision Science* **2019**, *96* (3), 180−186.
(42) Phan, C. M.; Walther, H.; Riederer, D.; Lau, C.; Lorenz, K. O.; Subbaraman, L. N.; Jones, L. Analysis of polyvinyl alcohol release from commercially available daily disposable contact lenses using an in vitro eye model. *Journal of Biomedical Materials Research Part B: Applied Biomaterials* **2019**, *107* (5), 1662−1668.
(43) Rizwan, M.; Peh, G. S.; Ang, H.-P.; Lwin, N. C.; Adnan, K.; Mehta, J. S.; Tan, W. S.; Yim, E. K. Sequentially-crosslinked bioactive hydrogels as nano-patterned substrates with customizable stiffness and degradation for corneal tissue engineering applications. *Biomaterials* **2017**, *120*, 139−154.
(44) Nakano, T.; Nakaoki, T. Coagulation size of freezable water in poly (vinyl alcohol) hydrogels formed by different freeze/thaw cycle periods. *Polym. J.* **2011**, *43* (11), 875−880.
(45) Procházková, L.; Rodríguez-Muñoz, Y.; Procházka, J.; Wanner, J. Simple spectrophotometric method for determination of poly-vinylalcohol in different types of wastewater. *International Journal of Environmental Analytical Chemistry* **2014**, *94* (4), 399−410.
(46) Liu, Y.; Fan, Q.; Huo, Y.; Liu, C.; Li, B.; Li, Y. Construction of a mesoporous polydopamine@ GO/cellulose nanofibril composite hydrogel with an encapsulation structure for controllable drug release and toxicity shielding. *ACS Appl. Mater. Interfaces* **2020**, *12* (51), 57410−57420.
(47) Elmas, A.; Akyüz, G.; Bergal, A.; Andaç, M.; Andaç, Ö. Mathematical modelling of drug release. *Res. Eng. Struct. Mater.* **2020**, *6* (4), 327.
(48) Madhavi, B.; Kusum, B.; Krishna Chatanya, C. H.; Madhu, M.; Sri Harsha, V.; Banji, D. Dissolution enhancement of efavirenz by solid dispersion and PEGylation techniques. *Int. J. Pharm. Invest.* **2011**, *1* (1), 29.
(49) Shakeel, A.; Bhattacharya, R.; Jeevanandham, S.; Kochhar, D.; Singh, A.; Mehra, L.; Ghufran, M.; Garg, P.; Sangam, S.; Biswas, S.; Tyagi, A.; Kalyanasundaram, D.; Chakrabarti, S.; Mukherjee, M. Graphene quantum dots in the game of directing polymer self-assembly to exotic kagome lattice and janus nanostructures. *ACS Nano* **2019**, *13* (8), 9397−9407.
(50) Li, H.; Wu, C.-w.; Wang, S.; Zhang, W. Mechanically strong poly (vinyl alcohol) hydrogel with macropores and high porosity. *Mater. Lett.* **2020**, *266*, No. 127504.
(51) Zeng, M.; Fang, Z.; Xu, C. Effect of compatibility on the structure of the microporous membrane prepared by selective dissolution of chitosan/synthetic polymer blend membrane. *J. Membr. Sci.* **2004**, *230* (1−2), 175−181.
(52) Adelnia, H.; Ensandoost, R.; Shebbrin Moonshi, S.; Gavgani, J. N.; Vasafi, E. I.; Ta, H. T. Freeze/thawed polyvinyl alcohol hydrogels: Present, past and future. *Eur. Polym. J.* **2022**, *164*, No. 110974.
(53) Labus, K.; Radosinski, L.; Kotowski, P. Functional Properties of Two-Component Hydrogel Systems Based on Gelatin and Polyvinyl Alcohol—Experimental Studies Supported by Computational Analysis. *International Journal of Molecular Sciences* **2021**, *22* (18), 9909.
(54) Jipa, I.; Stoica, A.; Stroescu, M.; Dobre, L. M.; Dobre, T.; Jinga, S.; Tardei, C. Potassium sorbate release from poly (vinyl alcohol)-bacterial cellulose films. *Chem. Papers* **2012**, *66*, 138−143.
(55) Aldana, A. A.; Malatto, L.; Rehman, M. A. U.; Boccaccini, A. R.; Abraham, G. A. Fabrication of gelatin methacrylate (GelMA) scaffolds with nano-and micro-topographical and morphological features. *Nanomaterials* **2019**, *9* (1), 120.
(56) Fonseca, D. F. S.; Costa, P. C.; Almeida, I. F.; Dias-Pereira, P.; Correia-Sá, I.; Bastos, V.; Oliveira, H.; Vilela, C.; Silvestre, A. J. D.; Freire, C. S. R. Swellable gelatin methacryloyl microneedles for extraction of interstitial skin fluid toward minimally invasive monitoring of urea. *Macromol. Biosci.* **2020**, *20* (10), 2000195.
(57) Velasco-Rodriguez, B.; Diaz-Vidal, T.; Rosales-Rivera, L. C.; García-González, C. A.; Alvarez-Lorenzo, C.; Al-Modlej, A.; Domínguez-Arca, V.; Prieto, G.; Barbosa, S.; Soltero Martínez, J. F. A.; et al. Hybrid Methacrylated Gelatin and Hyaluronic Acid Hydrogel Scaffolds. Preparation and Systematic Characterization for Prospective Tissue Engineering Applications. *Int. J. Mol. Sci.* **2021**, *22* (13), 6758.
(58) Pawde, S.; Deshmukh, K. Characterization of polyvinyl alcohol/gelatin blend hydrogel films for biomedical applications. *J. Appl. Polym. Sci.* **2008**, *109* (5), 3431−3437.
(59) Tozar, T.; Nistorescu, S.; Boni, M.; Gradisteanu Pircalabioru, G.; Negut, I.; Staicu, A. Pulsed Laser Photo-Crosslinking of Gelatin Methacryloyl Hydrogels for the Controlled Delivery of Chlorpromazine to Combat Antimicrobial Resistance. *Pharmaceutics* **2020**, *14* (10), 2121.

https://doi.org/10.1021/acsomega.4c08667
ACS Omega 2025, 10, 1249−1260

(60) El-Nemr, K. F.; Mohamed, H. R.; Ali, M. A.; Fathy, R. M.; Dhmees, A. S. Polyvinyl alcohol/gelatin irradiated blends filled by lignin as green filler for antimicrobial packaging materials. *International Journal of Environmental Analytical Chemistry* **2020**, *100* (14), 1578−1602.
(61) Shirahama, H.; Lee, B. H.; Tan, L. P.; Cho, N. J. Precise Tuning of Facile One-Pot Gelatin Methacryloyl (GelMA) Synthesis. *Sci. Rep-Uk* **2016**, *6*, No. 31036.
(62) Li, X. M.; Chen, S. W.; Li, J. C.; Wang, X. L.; Zhang, J.; Kawazoe, N.; Chen, G. P. 3D Culture of Chondrocytes in Gelatin Hydrogels with Different Stiffness. *Polymers-Basel* **2016**, *8* (8), 269.
(63) Wang, J.; Wang, X.; Liang, Z.; Lan, W.; Wei, Y.; Hu, Y.; Wang, L.; Lei, Q.; Huang, D. Injectable antibacterial Ag-HA/ GelMA hydrogel for bone tissue engineering. *Front Bioeng Biotechnol* **2023**, *11*, 1219460.
(64) Mehto, A.; Mehto, V. R.; Chauhan, J. Preparation and Characterization of Polyvinyl Alcohol (PVA)/ZrO2 Composite Membranes. *Phys. Status Solidi B* **2023**, *260* (10), 2300164.
(65) Song, X.; He, T.; Qi, Y.; Liu, Y.; Wu, H.; Liu, C.; Zhang, Y. Properties of cell-compatible poly (vinyl alcohol) hydrogels cross-linked with hydrophobic luteolin. *ACS Applied Polymer Materials* **2021**, *3* (6), 3019−3027.
(66) Wang, Y.; Wang, J.; Ma, Z.; Yan, L. A Highly Conductive, Self-Recoverable, and Strong Eutectogel of a Deep Eutectic Solvent with Polymer Crystalline Domain Regulation. *ACS Appl. Mater. Interfaces* **2021**, *13* (45), 54409−54416.
(67) Chen, L.; Qiang, T.; Chen, X.; Ren, W.; Zhang, H. J. Tough and biodegradable gelatin-based film via the synergistic effect of multi-cross-linking. *ACS Applied Polymer Materials* **2022**, *4* (1), 357−368.
(68) Ricciardi, R.; Auriemma, F.; Gaillet, C.; De Rosa, C.; Lauprêtre, F. Investigation of the crystallinity of freeze/thaw poly (vinyl alcohol) hydrogels by different techniques. *Macromolecules* **2004**, *37* (25), 9510−9516.
(69) Thomas, D.; Zhuravlev, E.; Wurm, A.; Schick, C.; Cebe, P. Fundamental thermal properties of polyvinyl alcohol by fast scanning calorimetry. *Polymer* **2018**, *137*, 145−155.
(70) Brazel, C. S.; Peppas, N. A. Mechanisms of solute and drug transport in relaxing, swellable, hydrophilic glassy polymers. *Polymer* **1999**, *40* (12), 3383−3398.
(71) Zhang, Y.; Sun, M.; Liu, T.; Hou, M.; Yang, H. Effect of different additives on the mechanical properties of gelatin methacryloyl hydrogel: a meta-analysis. *Acs Omega* **2021**, *6* (13), 9112−9128.
(72) Ahmed, L.; Atif, R.; Eldeen, T. S.; Yahya, I.; Omara, A.; Eltayeb, M. Study the using of nanoparticles as drug delivery system based on mathematical models for controlled release. *IJLTEMAS* **2019**, *8*, 52−56.
(73) Bruschi, M. L.*Strategies to modify the drug release from pharmaceutical systems*; Woodhead Publishing, 2015.
(74) Yu, J. R.; Janssen, M.; Liang, B. J.; Huang, H. C.; Fisher, J. P. A liposome/gelatin methacrylate nanocomposite hydrogel system for delivery of stromal cell-derived factor-1α and stimulation of cell migration. *Acta biomaterialia* **2020**, *108*, 67−76.

https://doi.org/10.1021/acsomega.4c08667
ACS Omega 2025, 10, 1249−1260